

Article type : Original Article

## Cathepsin C Modulates Myelin Oligodendrocyte Glycoprotein-induced Experimental Autoimmune Encephalomyelitis

Wilaiwan Wisessmith<sup>1,2,3,4,#</sup>, Takahiro Shimizu<sup>1,2,5,#</sup>, JiaYi Li<sup>1,2</sup>, Manabu Abe<sup>6</sup>, Kenji Sakimura<sup>6</sup>, Banthit Chetsawang<sup>3</sup>, Kenji F. Tanaka<sup>1,7</sup>, Suzumura Akio<sup>8</sup>, Koujiro Tohyama<sup>9</sup> and Kazuhiro Ikenaka<sup>1,2</sup>

1) *Division of Neurobiology and Bioinformatics, National Institute for Physiological Sciences, Okazaki, Japan.*

2) *Department of Physiological Sciences, SOKENDAI, Okazaki, Japan.*

3) *Research Center for Neuroscience, Institute of Molecular Biosciences, Mahidol University, Nakhonpathom, Thailand*

4) (Current affiliation) *Department of Pediatrics, University of Minnesota, Minneapolis, MN*

5) (Current affiliation) *Wolfson Institute for Biomedical Research, University College London, London, WC1E 6BT, UK.*

6) *Brain Research Institute, Niigata University, Niigata, Japan.*

7) *Department of Neuropsychiatry, Keio University, Tokyo, Japan.*

8) *Department of Neuroimmunology, Research Institute of Environmental Medicine, Nagoya University, Nagoya, Japan.*

9) *Department of Physiology, School of Dentistry, Iwate Medical University, Morioka, Japan*

# These authors contributed equally to the work.

This article has been accepted for publication and undergone full peer review but has not been through the copyediting, typesetting, pagination and proofreading process, which may lead to differences between this version and the Version of Record. Please cite this article as doi: 10.1111/jnc.14581

This article is protected by copyright. All rights reserved.

Address correspondence and reprint requests to Kazuhiro Ikenaka, PhD, 5-1 Aza-Higashiyama, Myodaiji, Okazaki, Aichi 444-8787, Japan. E-mail: ikenaka@nips.ac.jp

## Abstract

Multiple sclerosis (MS) is an autoimmune disease characterized by immune-mediated inflammation, which attacks the myelin sheath. MS pursues a relapsing and remitting course with varying intervals between symptoms. The main clinical pathological features include inflammation, myelin sheath destruction and plaque formation in the central nervous system (CNS). We previously reported that cystatin F (CysF) expression is induced in demyelinating lesions that are accompanied by active remyelination (referred to as shadow plaques) but is down regulated in chronic demyelinated lesions (plaques) in the spinal cord of MS patients and in several murine models of demyelinating disease. CysF is a cathepsin protease inhibitor whose major target is cathepsin C (CatC), which is co-expressed in demyelinating regions in *Plp<sup>4e/-</sup>* mice, a model of chronic demyelination. Here, we report the time course of *CatC* and *CysF* expression and describe the symptoms in a mouse experimental autoimmune encephalomyelitis (EAE) model using *CatC* knockdown (KD) and *CatC* overexpression (OE) mice. In myelin oligodendrocyte glycoprotein (MOG)-EAE, *CatC* positive cells were found to infiltrate the CNS at an early stage prior to any clinical signs, in comparison to WT mice. *CysF* expression was not observed at this early stage, but appeared later within shadow plaques. *CatC* expression was found in chronic demyelinated lesions but was not associated with *CysF* expression, and *CatCKD* EAE mouse showed delayed demyelination. Whereas, *CatCOE* in microglia significantly increased severity of demyelination in the MOG-EAE model. Thus, these results demonstrate that *CatC* plays a major role in MOG-EAE.

**Keywords:** Demyelination, Cathepsin C, Cystatin F, experimental autoimmune encephalomyelitis (EAE), multiple sclerosis.

Abbreviations used: BBB, blood–brain barrier; *CatC*, cathepsin C; CNS, central nervous system; *CysF*, cystatin F; EAE, experimental autoimmune encephalomyelitis; KD, knockdown; MBP, myelin basic protein; MOG, myelin oligodendrocyte glycoprotein; MS, multiple sclerosis; OE, overexpression; *Plp<sup>4e/-</sup>*, hemizygous proteolipid protein 1 transgenic mouse strain, 4e; WT, wild type; H&E, hematoxylin and eosin; ISH, in situ hybridization; IHC, immunohistochemistry; Gal3, galectin-3; PLP, proteolipid protein; RRID, Research Resource Identifier.

## Introduction

Multiple sclerosis (MS) is an immune-mediated disease accompanied by demyelination that affects the CNS, and is the most common cause of serious physical disability in young adults, especially in women. It is believed that the demyelination is caused by an immune system attack, and relapses coincide with focal CNS inflammation and demyelination (Dendrou *et al.* 2015). It is thus important to prevent aggravation during the early stages of MS and to elucidate the causes of aggravation.

Experimental autoimmune encephalomyelitis (EAE) is induced by autoimmune reaction against myelin components and is the most commonly used experimental animal models for inflammatory demyelinating disease, such as MS, as it shows similar clinical and histological features (Robinson *et al.* 2014, Baker & Jackson 2007, Lampron *et al.* 2015). However, myelin oligodendrocyte glycoprotein (MOG)-EAE mice gain full recovery over time, which is different from relapse-remitting MS. (McPherson *et al.* 2014, Nuro-Gyina *et al.* 2016). Neuroprotective microglia/macrophage cells are found more than damaging microglia/macrophage cells during the early phase in acute EAE but damaging microglia/macrophage cells become abundant during peak and recovery phase of EAE (Ahn *et al.* 2012). Damaging macrophages/microglia usually secrete pro-inflammatory cytokines and neuroprotective macrophages/microglia usually secrete anti-inflammatory cytokines (Martinez *et al.* 2009, Hind *et al.* 2016). Previous studies showed that the microenvironment of severe relapsing EAE prefer polarization to damaging cells and increasing the number of neuroprotective cells would be supportive for the treatment of this disease (Cao & He 2013).

In previous studies from our group, using the hemizygous proteolipid protein 1 transgenic mouse strain, 4e (*plp<sup>4e/-</sup>*), a chronic demyelinating model, we showed that cystatin F (CysF) gene expression increases at the acute demyelinating and remyelinating stages but is rapidly decreased when remyelination is impaired in chronic phase (Ma *et al.* 2007, Ma *et al.* 2011, Shimizu *et al.* 2017). CysF is a papain-like lysosomal cysteine proteinase inhibitor, also known as Cst7, CMAP (cystatin-like metastasis-associated protein) and leukocystatin. CysF is selectively expressed in immune cells. The major target of CysF is cathepsin C (CatC), which is a lysosomal cysteine protease also known as Ctsc, DPPI, DPP1 and AI047818 (Hamilton *et al.* 2008). The function of CatC is to cleave dipeptides from the amino terminal of various peptides and proteins, and to activate many granule-associated serine proteases that associate with inflammatory and immune response processes, such as neutrophil elastase, the cytotoxic lymphocyte-associated protease, granzymes A and B and neutrophil-derived cathepsin G (Pham & Ley 1999, Adkison *et al.* 2002). A previous study showed that CatC is the primary enzyme that activates neutrophil-derived serine proteases *in vivo*. These proteases are very important for inflammatory processes, and the CatC deficiency dramatically protected against arthritis development in a model of acute inflammatory arthritis (Adkison *et al.* 2002, Eyles *et al.* 2006).

In our previous study, we found that *CysF* knockdown (KD) or *CatC* overexpression (OE) in microglia exacerbate the demyelinating symptoms in *plp<sup>4e/-</sup>* mice (Shimizu *et al.* 2017). A similar result was found in a cuprizone-induced demyelination model, where the absence of the *CysF* gene and the resulting disinhibition of *CatC* aggravated the demyelination (Liang *et al.* 2016). *CatC* activity can be regulated by various mechanisms and is involved in inflammatory responses (Conus & Simon 2008); for example, the absence of the *CysF* gene increases the activity of *CatC* and enhances demyelination. These studies demonstrated that *CatC* and *CysF* are strongly associated with demyelinating processes including the prevention of demyelination. The *plp<sup>4e/-</sup>* mouse is a useful model for chronic demyelination phase of MS because it has a similar pathology to MS in the late phase. Conversely, *plp<sup>4e/-</sup>* mice are not suitable for studying the acute phase of demyelination because the disease mechanism is different from MS, e.g. it occurs without T-cell infiltration. The cuprizone model is also used to study the acute demyelination phase of MS. However, unlike MS, the cuprizone model maintains an intact blood-brain barrier (BBB) with no T-cell infiltration. Thus, we utilized the MOG-EAE model to study the acute demyelination phase. Here, we investigated the expression patterns of *CatC* and *CysF* in the MOG-EAE model using wild type (WT) mice and characterized the symptoms in *CatCKD* and *CatCOE* MOG-EAE mice both clinically and histologically. We found that *CatC* is expressed in demyelinating lesions and that *CysF* is expressed in shadow plaques of MOG-EAE WT mice spinal cord. *CatC* was expressed in the chronic demyelinating area where myelin is completely lost. Conversely, *CysF* was expressed in the area surrounding the chronic demyelinated area. We also found that *CatC* plays a role in aggravating the symptoms in MOG-EAE. These results suggest that *CatC* is a potential target for suppressing the progression of demyelination during the early phase of EAE.

## Materials and Methods

### Experimental Animals

The Neo STOP-tetO insertion cassette containing 10 kb of the targeting vector (3' homology arm), 1.8 kb of Neo STOP-tetO cassette (5' homology arm) and diphtheria toxin A was inserted upstream of *CatC* translation initiation site (Shimizu *et al.* 2017). The C57BL/6N ES cell line RENKA (Mishina and Sakimura 2007) was used for the recombination. The *CatC<sup>STOPtetO</sup>* mouse line (generated using the FAST system) and *Iba1-tTA* mouse line 75 (initial BDF1 background backcrossed to C57BL/6 background; Tanaka *et al.*, 2012) were used to generate *CatC* overexpressing mice (*CatC<sup>STOP/+</sup>::Iba1<sup>tTA/+</sup>*; *CatCOE*) and *CatC* knockdown mice (*CatC<sup>STOP/STOP</sup>*; *CatCKD*) and C57BL/6N (Charles River, Yokohama, Japan, C57BL/6Ncrl) mice were used in this study (Tanaka *et al.* 2010, Shimizu *et al.* 2017). Mouse genotyping was performed using following PCR primer sets: two pairs of primers, *CatC205L* (5'-AAGGCAAGGACTCAGGGACAGAAA-3') and *tetOup* (5'-AGCAGAGCTCG-TTTAGTGAACCGT-3') were used for the knock-in allele of the *CatCSTOP-tetO* mouse; *CatC361U* (5'-TTTGGCGTTCCTTGAAAGGCAGAG-3') and *CatC205L* (5'-AAGGCAAGGACTCAG-GGACAGAAA-3') for the wild type allele of the *CatC* gene; *CysF708L* (5'-TCTCAGGGTTCCAAGAGTGTCC-3'); *Iba1552U* (5'-

ATGCCTGGGAGTTAGCAA-GGGAAT-3') and mTA24L (5'-CGGAGTTGATCACCTTGGACTTGT-3') for the Iba1-mTA mouse. To detect the CatC WT allele, we used CatC361U and CatC205L, with a PCR product size of 566 bp. To detect the CatC STOP-tetO KI allele, we used tetOup and CatC205L, with a PCR product size of approximately 340 bp.

All animal procedures were conducted in accordance with the guidelines described in the National Institutes of Health Guide for the care and use of laboratory animals, and by the National Institute for Physiological Sciences Animal Care and Use Committee (approval # 10A250). All efforts were made to minimize distress and pain. The generation of STOPtetO mice was conducted in accordance to the animal welfare committees and the ethics committees of Niigata University guideline. All animals were kept on a 12:12 hours light/dark cycle housed with no more than 4 adult mice per cage with food and water available *ad libitum*.

#### Myelin oligodendrocyte glycoprotein induced experimental autoimmune encephalomyelitis (MOG-EAE)

Mice (n = 55; age 7 to 10 weeks) weighing between 18 to 22 g were used for this experiment. The overview of the study design is described in Fig. 1. Mice of both sexes were used in this study. The study was not pre-registered. No randomization procedures nor sample size calculation were performed in this study. The MOG<sub>35-55</sub> peptide; MEVGWYRSPFSRVVHLYRNGK (150 µg; Custom made, Peptide Institute Inc., Osaka, Japan) was emulsified in complete Freund's adjuvant (CFA; Sigma-Aldrich, Missouri, USA, F5581) consisting with 1:1 ratio of incomplete Freund's adjuvant (IFA; Sigma-Aldrich, Missouri, USA, F5506) and Mycobacterium tuberculosis 4 mg/ml (Difco Laboratories, Detroit, MI, USA, 231141). Mice were subcutaneously immunized with MOG/CFA into two sites of dorsal flank followed by an intraperitoneal injection with pertussis toxin (400 ng; List Biological Labs, Inc., CA, USA, #180) at day 0 (immediately after immunization) and day 2 (48 hours later). The WT MOG EAE mice were observed daily and tissues collected at 1, 2, 3, 4 and 6 weeks after immunization for analysis (n = 3 per each group, total n = 15 mice; Fig. 2A). Transgenic mice (CatCKD, CatCOE and WT) were monitored daily until day 14, but some mice were euthanized earlier to collect tissue for analysis (Fig. 1). The samples for tissue analysis were collected at the beginning of EAE on day 10 (n = 9), day 12 (n = 9) and peak EAE on day 14 (n = 22) after immunization (total n = 40 mice).

The clinical phenotype of EAE was monitored daily and given a clinical score: clinical score range from 0-5 and are based on disease severity: 0, no clinical signs; 1, limp tail; 1.5, impaired righting reflex and limp tail; 2, limp tail and v d' j ndr r hmhindlimbs; 2.5, limp tail and paralyzed one of the hindlimbs; 3, o` q kycdc both hindlimbs or one r h d ne enqdkl a and

hindlimb or the combination of all of the following symptoms - spinning when picked up by the tail+severe head tilting, walking by pushing body along edges against to the cage wall; 3.5, completely paralyzed ansg ne hindkl ar; 4, completely paralyzed of both hindlimbs and one fnqkl a; 5, complete quadriplegia, moribund or death of the animal. In addition, any animals that reached the peak of EAE pathology and died were given a score of five.

Experimental lists of genotypes were blinded during the investigation to minimize potential bias. Mice also were observed for pain and discomfort signs from EAE during daily monitoring (abnormal appearance, altered behavior, vocalization, mutilation and inappetence). Those mice which suffered from EAE clinical phenotype were separated and granted easier access to water and food. Mice that reached a moribund stage and are moribund with EAE should be sacrificed for humane reasons. The data should be excluded if mice showed no clinical phenotype (score 0), indicating unsuccessful MOG-EAE, or were sick/moribund without any EAE-related clinical phenotype. No mice were excluded in this study based on the described exclusion criteria. No pain medications were applied in this study.

#### Mouse tissue preparation

Mice were anesthetized by intraperitoneal injection of chloral hydrate and anesthesia result was assessed by the complete depression of palpebral and pedal reflexes. Mice were perfused with phosphate-buffered saline (PBS), followed by 4% paraformaldehyde (PFA) in PBS through cardiac puncture. Brains and thoracic spinal cords were dissected out and post-fixed in the same fixative overnight. The tissues were then cryoprotected with PBS containing 20% sucrose overnight and embedded in OCT compound (Sakura Finetek Co., Tokyo, Japan, 4583). Sections were cut at a thickness of 20  $\mu\text{m}$  with a cryostat (Leica CM3050, Germany).

#### *In Situ* hybridization

Frozen sections of spinal cord that had been perfused with 4% PFA were used. These were postfixed for 20 minutes in 4% PFA, washed with PBS twice for 5 minutes, and treated for 30 minutes with 20  $\mu\text{g/ml}$  proteinase K. To inactivate proteinases, sections were briefly washed with PBS and then fixed with 4% PFA for 15 minutes. Sections were further washed with 0.1 M triethanolamine-HCl for 15 minutes and washed with PBS twice for 5 minutes. Pre-hybridization was carried out for 2-4 hours at 65°C in hybridization buffer (5X saline-sodium citrate (SSC), 50% formamide, 200  $\mu\text{g/ml}$  heparin and 0.2 mg/ml yeast tRNA). Hybridization was conducted at 65°C overnight. Hybridization buffer contained 300 ng/ml digoxigenin labeled cRNA probe. Sections were washed with SSC and blocked with blocking buffer followed by alkaline phosphatase conjugated anti-digoxigenin antibody incubation at

room temperature for 60 minutes. Un-bound antibody was removed by washing with MABT solution (100 mM maleic acid, 150 mM NaCl, 0.1% Tween20, pH 7.5) for 30 minutes, 3 times. Nitro blue tetrazolium chloride/5-bromo-4-chloro-3-indolyl phosphate (NBT/BCIP) (Roche diagnostics, Germany, 11681451001) was used to develop color for up to 24 hours and then NBT/BCIP reaction stopped by washing remaining solution with PBS. Nuclear Fast Red (Vector Lab, Burlingame, CA, H-3403) was used as counterstaining solution. The Olympus digital camera system (DP70) in combination with an Olympus BX51 microscope was used to capture images.

### Immunohistochemical Analysis

Frozen sections of spinal cord that had been perfused with 4% PFA were used. Washing the thoracic spinal cord cryosections with PBS for 5 min was followed by antigen retrieval with citrate buffer. Tissue slides were treated with citrate buffer 10 mM (pH 6.0) and heated in a microwave oven (550W) for 3 min, then sections were left until they cooled down. The sections were treated with 0.03% H<sub>2</sub>O<sub>2</sub> in 0.1% Triton-X100 PBS-T for 30 minutes and washed with PBS 3 times for 5 minutes. Normal goat serum (10%) in PBS-T was used as blocking agent to reduce non-specific binding. The sections were blocked at room temperature for 60 minutes, followed by primary antibodies incubation at 4°C overnight. After washing with PBS 3 times, sections were incubated with secondary antibodies at room temperature for 60 minutes, washed with PBS-T three times for 5 min and then incubated with horseradish peroxidase streptavidin biotin complex or ABC solution (Vector laboratories, CA, USA, PK-4000; RRID:AB\_2336818). The color development was performed with 3,3'-diaminobenzidine (DAB) solution (Vector laboratories, CA, USA, SK-4100; RRID:AB\_2336382) with 0.03% H<sub>2</sub>O<sub>2</sub>. The sections were dehydrated with ethanol in 70%, 80%, 90%, 100% serial concentrations, respectively. The sections were cleared with Clear Plus and were mounted with PermOUNT solution. The Olympus digital camera system (DP70) in combination with an Olympus BX51 microscope was used for capturing images. The following antibodies were used; rabbit polyclonal anti-Iba1 antibody (1:1000; Wako, Osaka, Japan; RRID:AB\_2665520), polyclonal goat anti-arginase-1 antibody (1:200; Santa Cruz Biotechnology, CA, USA; RRID:AB\_2058955), monoclonal rat anti-CD16/32 antibody (1: 200; Santa Cruz Biotechnology, CA, USA; RRID:AB\_2103884) and rat anti-PLP/DM20 antibody (1:10; AA3 hybridoma cell culture supernatant gifted by Dr. Lees M. B). Biotinylated antibodies were used as secondary antibody. After washing off the unbound secondary antibody, sections were incubated with Vectastain ABC HRP kit (RRID: PK-4000, Vector laboratories, CA, USA) for calorimetric development. The secondary antibodies below were used. Biotinylated goat anti-rat IgG antibody (1:200; RRID: BA-9400, Vector laboratories, CA, USA), biotinylated goat anti-rabbit IgG antibody (1:200, RRID:BA-1000, Vector laboratories, CA, USA).

For immunofluorescence, cryosections from spinal cords perfused with 4% PFA were used. The sections were briefly washed with PBS for 5 minutes, followed by antigen retrieval process and then washed again with PBS (3 times for 5 minutes). The sections were blocked with blocking agent to reduce non-specific binding at room temperature for 60 minutes, followed by primary antibody incubation at 4°C overnight. Appropriate Alexa-conjugated secondary antibodies; Alexa 568-conjugated anti-mouse IgG (Invitrogen; RRID:AB\_141611) and Alexa 568-conjugated anti-rat IgG (Invitrogen; RRID:AB\_141874) were used.

### Electron microscopy

Mice were perfused with fixative solution which contained 2.5% (v/v) glutaraldehyde and 2.0% (w/v) PFA in 0.1 M cacodylate buffer (pH 7.4) into mouse circulation through the left ventricle. Spinal cord were immersed in the fixative solution for a couple of days at 4°C, then 0.5 mm thick cross section slices of spinal cord were prepared with a razor blade and 2 mm x 1.5 mm blocks were further processed for electron microscopy.

The specimens were immersed in 1% (w/v) osmium tetroxide solution for 2 hours at 4°C, followed by dehydration process through a graded alcohol series and embedded in Epon 812 resin (TAAB Laboratories, Aldermaston, UK, T022). The specimens were collected for 1 µm semithin section, stained with toluidine blue 0.5% (w/v) in 0.1 M PB and images were captured with an Olympus light microscope equipped with an auto-digitizer to generate “virtual slides” (NanoZoomer-RS, Hamamatsu Photonics). The ultrathin sections were collected for whole area EM analysis of the same specimens by ultra-microtome (Ultracut UCT, Leica, Germany) without trimming on platinum-coated glass slides, stained with uranyl acetate and lead citrate. The specimen grids were imaged with a scanning electron microscope equipped with a back-scattered electron beam detector (SU8010, Hitachi, Japan) at 1.5 KV accelerating voltage. From each section, a digitized image with an area of about 200 µm by 300 µm was captured at a resolution of 24.8 nm/pixel.

### Image and Statistical Analysis

The total myelin stained areas were quantified by densitometric analysis with Image J program (National Institutes of Health, Bethesda, MD, USA; RRID:SCR\_003070). Data was represented in the mean  $\pm$  S.E.M. The significance was assessed by an unpaired two-tailed Student's *t*-test, one-way or two-way analysis of variance (ANOVA) followed by a Bonferroni test using the scientific statistics software Graphpad Prism version 5.0b (GraphPad Software, Inc., La Jolla, CA, USA; RRID:SCR\_002798). *P*-values were considered significant when less than 0.05. The test for outliers was not conduct on the data.

## Results

*CatC* and *CysF* expression patterns in the spinal cord of MOG-EAE mice at different time points.

In previous studies using *Plp<sup>4e/-</sup>* mice, a chronic demyelination model, *CatC* and *CysF* expression were demonstrated in specific patterns; *CysF* dominated *CatC* during the remyelination, then *CatC* dominated *CysF* during the chronic demyelination. However, *Plp<sup>4e/-</sup>* mice and cuprizone model mice do not show inflammation associated with T-cell infiltration, which is a critical difference from the acute phase of MS. Thus, MOG-EAE was chosen as a model to study inflammatory demyelination in early phase because of the similarities with early phase MS. *CatC* and *CysF* expression was examined in the spinal cord of MOG-EAE mice. We generated the MOG-EAE model using WT mice and observed the distribution of *CysF* and *CatC* mRNA in the spinal cord at 1, 2, 3, 4 and 6 weeks after immunization (Fig. 2A). MOG-EAE mice were observed for clinical signs every day after immunization and were recorded as clinical scores until the day of sacrifice.

One week after immunization (Fig. 2B), mice showed no clinical signs (clinical score = 0) and demyelination was not found in the spinal cord (Fig. 2B4). Surprisingly, *CatC* mRNA positive cells were found in the gray matter and white matter, and were found infiltrated into the anterior median fissure of the spinal cord (Fig. 2B1) where *c-fms* mRNA-positive cells were accumulated (Fig. 2B3). In contrast, *CysF* mRNA-positive cells were not found at this stage (Fig. 2B2). Two weeks after immunization (Fig. 2C), mice started to show clinical signs, including a limp tail and gradual progressive weakness of the hindlimbs and a disturbance of the righting reflex (clinical score = 2/3). At this stage, demyelinating lesions were observed based on PLP immunostaining (Fig. 2C4, area surrounded by the broken red line). The accumulation of more *CatC* and *c-fms* mRNA-positive cells were observed in the demyelinating area (Fig. 2C1 and 3), whereas few *CysF* mRNA-positive cells were found at the demyelinating area edge, where myelin remained. Three to four weeks after immunization (Fig. 2D-E), many demyelinating lesions were clearly shown, and mice established severe clinical signs (clinical score = 3/4), including paralysis in both hind limbs. *CatC* and *c-fms* mRNA-positive cells were found aggregated largely in the demyelinating and surrounding areas. *CysF* expression remained at weak levels and *CysF*-positive cells were only observed in the shadow plaques. Clinical scores gradually declined 6 weeks after immunization. At this stage, demyelinating lesions became smaller (Fig. 2F4) and *CatC* and *c-fms* positive cells were found only in a small region of spinal cord, where demyelination is observed (Fig. 2F1 and 3). *CysF* mRNA-positive cells were distributed in a similar pattern to that of *CatC*-positive cells, although it was only found in the shadow plaques (Fig. 2F2). The percentage of demyelinated area in spinal cord increased over time after immunization, which started at two weeks after immunization (Fig. 2G). The percentage of the demyelinating area at four weeks after immunization significantly increased ( $4.35 \pm 0.71$  %;  $n = 3$ ) compared to that of one week after immunization group (0%;  $n = 3$ ) ( $p < 0.001$ ), two weeks after immunization group ( $1.82 \pm 0.42$  %;  $n = 3$ ) ( $p < 0.05$ ), however no significant difference was

found when compared to three weeks after immunization group ( $2.99\% \pm 0.32\%$ ;  $n = 3$ ). The percentage of the demyelinating area at six weeks after immunization significantly decreased ( $1.16 \pm 0.13\%$ ;  $n = 3$ ) ( $p < 0.01$ ) compared to that of four weeks after immunization group.

We found *CatC* mRNA-positive infiltrating cells in the anterior median fissure during the very early phase (the 1<sup>st</sup> week after immunization) of MOG-EAE when there are no obvious demyelinating lesions nor physical signs. *CatC* mRNA-positive infiltrating cells were found in the white matter through the end of the observation period 6 weeks after immunization. *CysF* mRNA-positive cells were found later than *CatC*-positive cells in the shadow plaques.

To identify the cell types expressing *CatC* mRNA during the early stage, MOG-EAE mice were examined at one week after immunization. The results showed that the *CatC* mRNA-positive cells in the anterior gray horn of the spinal cord were microglia, and not infiltrating T cells (Fig. 3A and C). The *CatC* mRNA-positive cells, which infiltrated at the anterior median fissure may associated with hematopoietic cell lineages which crossed the blood–brain barrier (BBB) after triggering an immune reaction caused by EAE. The infiltrating cells type was identified as polymorphonuclear based on cell morphology, which identifies them as neutrophil granulocytes (Fig. 3D). *CatC* ISH showed that most of the cells at the median anterior fissure of the spinal cord were *CatC* mRNA-positive (Fig. 3B). In summary, *CatC* mRNA-positive cells were found in the microglia at the anterior gray horn and in the infiltrating cells (including neutrophils) at the anterior median fissure of the spinal cord.

Expression of *CatC* and *CysF* mRNA in regions of degenerated myelin.

Myelin debris phagocytosis in acute MS lesions by microglia and macrophages is well studied, and the immune system is the primary mechanism that is used to remove cell debris and pathogens (Liu *et al.* 2006). *CatC* mRNA-positive cells were the only cells that were observed to be infiltrating the CNS prior to triggering myelin damage by an immune attack in the early phase of EAE. However, we did not find any *CysF* involvement in this phase (Fig. 2). *CatC* and *CysF* expression was also observed at a later stage of EAE, when immune attack induced myelin degeneration and myelin debris phagocytosis that was labeled by *galectin 3* (*Gal3*) ISH (Sano *et al.*, 2003) (Fig. 4A). The demyelinated lesions were found after two weeks of immunization (Fig. 4B). *CatC* and *Gal3* mRNA-expressing cells were also found in the demyelinated area of the anterior funiculus (Fig. 4A, B and C). Weaker *CysF* ISH signals were found in the chronic demyelinated region (Fig. 4D). These results suggest that *CatC* plays a role during microglia/macrophages phagocytosed myelin sheaths. Moreover, this also suggests that *CysF* plays a lesser role in the late inflammatory demyelinating phase of MOG-EAE, as *CysF* expression was much lower than *CatC* in the

mid-stage of inflammation in MOG-EAE, when mice showed severe physical signs (clinical score 3, 4 and 5).

## Neuroprotective and damaging microglial polarization in MOG-EAE inflammatory demyelination

Macrophage/microglial polarization, which consists of pro-inflammatory damaging (M1) or anti-inflammatory neuroprotective (M2) subtypes, plays a central role in the response to spinal cord inflammation. Previous studies showed that neuroprotective polarization appeared in injured spinal cord microenvironment, in which damaging macrophages transiently appeared only in an early stage after injury (David & Kroner 2011). Neuroprotective and damaging macrophage/microglial cells were observed in MOG-EAE mice. Thoracic spinal cord sections from the WT mice were analyzed 6 weeks after immunization for the expression of neuroprotective or damaging macrophage/microglial markers in cells of the demyelinating lesions. Damaging cells were found to aggregate in the demyelinating regions (Fig. 5A-C) but only a small number of neuroprotective macrophage/microglial cells were observed (Fig. 5D-F).

CatC plays a role during the early phase of the inflammatory demyelinating model.

We discovered that the *Plp1*-overexpressing mouse line (*Plp*<sup>4e/-</sup>) and cuprizone mouse model showed worsened symptoms in our previous studies when *CysF* expression was eliminated, indicating that *CysF* has supporting role in the demyelinating mouse models which do not show hematopoietic cell infiltration in the lesions (Liang *et al.* 2016, Shimizu *et al.* 2017). In that previous study, the balance between *CatC* and *CysF* expression was shown to be essential for myelin regeneration maintenance in both the early and chronic phase of *Plp*<sup>4e/-</sup> mice. In conclusion, *CatC* might also have an essential part in demyelinating or myelin regenerating processes during the early immune attacking stage in MOG-EAE. To examine the role of *CatC*, cathepsin C knockdown (CatCKD) and WT mice were used for MOG-EAE. The clinical scores of MOG-EAE CatCKD mice were significantly lower than those of WT mice 10 and 11 days after the immunization (Fig. 6A), suggesting that *CatC* expression is toxic to the mice during MOG-EAE. To confirm this, cathepsin C-overexpressing (CatCOE) and WT mice were used for MOG-EAE. The clinical scores of CatCOE mice were significantly higher than for WT mice between the 7<sup>th</sup> and 14<sup>th</sup> days after immunization (Fig. 6B).

CatCKD, CatCOE and WT mice were further analyzed histologically at two weeks after immunization. CatCOE mice and the WT mice appeared to have similar expression pattern of *CatC* mRNA positive cells, which were found to infiltrate the CNS (Fig. 7A1-C1). The low levels of *CysF* mRNA positive cells were observed around demyelinating area (Fig. 7A2-C2). The activated microglial, which were labeled by *c-fms* mRNA signals was

observed in the demyelinating region (Fig. 7A3-C3). CatCOE EAE mice showed a significantly larger demyelinating area than the control group; conversely, CatCKD EAE mice showed a significant decreased demyelinating area compared to the control group (Fig. 7A4-C4, 7D). The percentage of the demyelinating area in CatCOE mice significantly increased ( $4.23 \pm 0.24$  %;  $n = 4$ ) compared to that of the control ( $2.88 \pm 0.49$  %;  $n = 4$ ) group ( $p = 0.0492$ ). However, no significant difference was found between CatCKD ( $1.18 \pm 0.38$  %;  $n = 3$ ), and WT EAE mice ( $p = 0.0512$ ). These results are consistent with previous data using *Plp<sup>4e/-</sup>* and cuprizone model mice (Liang *et al.* 2016, Shimizu *et al.* 2017), suggesting that CatC plays a role during the early stage of inflammatory demyelinating disease.

Representative electron micrographs of thoracic spinal cords from CatCOE, CatCKD and WT MOG-EAE mice were observed 12 days after immunization (Fig. 8). The CatCOE EAE mice showed multinuclear cells (neutrophils) invading into the white matter of the spinal cord (Fig. 8C, F). However, these cells were not found in CatCKD EAE (Fig. 8B, E) or WT EAE mice (Fig. 8A, D). The number of the multinuclear invading cells in CatCOE mice significantly increased ( $7 \pm 1.15$  %;  $n = 3$ ) ( $p < 0.001$ ) when compared to that of CatCKD (0;  $n = 3$ ) and WT EAE (0;  $n = 3$ ) (Fig.8G).

## Discussion

In this study, using the MOG-EAE model, CatC was demonstrated to play an important role in inflammatory demyelination. First, CatC-expressing cells, which include neutrophils and microglia, infiltrate the CNS during EAE in the early stage, prior to the observation of any clinical signs. Previous studies indicated that the neutrophils, which are one of the inflammatory cells was significantly increased during the disease onset and initiate EAE. These suggest that neutrophils play an important role in EAE pathogenesis and may contribute to demyelinating process in EAE acute phase (Wu *et al.* 2010, Nemeth *et al.* 2016). Neutrophils also have role to assist the blood-brain barrier breakdown, combined with T cells, resulting in influx of inflammatory cells and cause myelin damage (Sayed *et al.* 2010). CatC activates some proteases such as cathepsin G (CatG), proteinase 3 (PR3) neutrophil-derived serine proteases and neutrophil elastase (NE), which are specifically found in mature neutrophils, and plays an essential role in inflammation (Adkison *et al.* 2002). Neutrophils are also shown to be a source of CatC secretion during inflammatory processes (Hamon *et al.* 2016). Moreover, CatC is mostly found in activated microglial cells throughout the brain in early phase of neuroinflammation, which is induced by lipopolysaccharide (LPS) (Fan *et al.* 2012). These evidences propose that CatC is one of the factors in the progression of neuroinflammation and develop demyelination in the CNS.

*CatC-CysF* were shown to prolong expression along the demyelination process in MOG-EAE. *CatC* was found in chronic demyelinated regions, where the myelin regenerating process has ceased; in contrast, *CysF* was found at the demyelinated lesion edge, where myelin remained intact. *CatC* is one of the two genes out of 12,000 that were found to be constantly upregulated during the first couple weeks of MOG-EAE (Mix *et al.* 2004). T lymphocytes, the mediators of EAE, enter the CNS parenchyma, which is the critical early event in the immune-mediated illnesses pathogenesis (Zamvil & Steinman 1990, Flach *et al.* 2016). *CatC* is involved in the granzyme processing, which is a neutral serine protease specifically found in activated cytotoxic lymphocytes granules (Kummer *et al.* 1996, Pham & Ley 1999). Active forms of granzyme will activate several downstream cascades, such as pro-inflammatory cytokines TNF- $\alpha$  and IL-1 $\beta$  induction or cell death pathway (Shresta *et al.* 1999, García-Laorden *et al.* 2016). The pro-inflammatory damaging (M1) macrophages, induced by TNF $\alpha$ , were present in the chronic demyelinated region and correlated with *CatC* expression (Sindrilaru *et al.* 2011). *CatC* may promote neurodegenerative (M1) polarization, which causes inhibition of regeneration process in myelin sheath (David & Kroner 2011). Reducing the cytokine levels and other factors in the damaged spinal cord microenvironment responsible for prolonged or excessed neurodegenerative are likely a promising therapeutic target.

A similar *CysF* mRNA-expression pattern was found in the chronic demyelination model, *Plp*<sup>4e/-</sup> mouse, as in the EAE mouse model: expression decreased when remyelination was severely affected at age 8 months (Shimizu *et al.* 2017). *CysF* was identified as an ongoing remyelination indicator in various demyelinating models (Ma *et al.* 2011). The result from MOG-EAE induction in *CatCKD* and *CatCOE* mice in this present study confirmed that *CatC* and *CysF* are strongly associated with inflammatory demyelination. The severity of EAE was reduced in the absence of *CatC*, whereas increased microglial *CatC* expression enhanced clinical severity (Fig. 6, 7 and 8). These results strongly propose that the interaction of *CatC-CysF* plays an essential role in the inflammatory demyelination pathogenesis of EAE.

EAE is most commonly used animal model for MS and other demyelinating diseases. The possible role of *CatC* and *CysF* in the inflammatory demyelination model was examined in this study. The discovery of a *CatC* and *CysF* system might be key to develop new treatments in the future.

--Human subjects --

Involves human subjects:

If yes: Informed consent & ethics approval achieved:

=> if yes, please ensure that the info "Informed consent was achieved for all subjects, and the experiments were approved by the local ethics committee." is included in the Methods.

--Acknowledgments--

This work was funded by Thailand Research Fund under the Royal Golden Jubilee-Ph.D. Scholarship and Mahidol University, (Grant / Award Number: ) Foundation of Synapse and Neurocircuit Pathology, (Grant / Award Number: '23110521') Glial Assembly: a new regulatory machinery of brain function and disorders, (Grant / Award Number: '25117001') (grant number ): This information is usually included already, but please add to the Acknowledgments if not.

ARRIVE guidelines have been followed:

Yes

=> if No or if it is a Review or Editorial, skip complete sentence => if Yes, insert "All experiments were conducted in compliance with the ARRIVE guidelines." unless it is a Review or Editorial

Conflicts of interest: The authors declare a conflict of interest that Kazuhiro Ikenaka is the current president of the ISN.

=> if 'none', insert "The authors have no conflict of interest to declare."

=> otherwise insert info unless it is already included

## Acknowledgements and conflict of interest disclosure

This work was supported by Grants-in-Aid for Scientific Research on Innovative Areas: "Foundation of Synapse and Neurocircuit Pathology (23110521)" to KI, Japan Society for the Promotion of Science (JSPS), "Glial Assembly: a new regulatory machinery of brain function and disorders (25117001)" to KI and "Thailand Research Fund under the Royal Golden Jubilee-Ph.D. Scholarship and Mahidol University" to WW and BC. The authors declare a conflict of interest that Kazuhiro Ikenaka is the current president of the ISN.

## References

Adkison, A. M., Raptis, S. Z., Kelley, D. G. and Pham, C. T. (2002) Dipeptidyl peptidase I activates neutrophil-derived serine proteases and regulates the development of acute experimental arthritis. *J Clin Invest*, **109**, 363-371.

- Ahn, M., Yang, W., Kim, H., Jin, J. K., Moon, C. and Shin, T. (2012) Immunohistochemical study of arginase-1 in the spinal cords of Lewis rats with experimental autoimmune encephalomyelitis. *Brain Res*, **1453**, 77-86.
- Baker, D. and Jackson, S. J. (2007) Models of Multiple Sclerosis. *Adv Clin Neurosci Rehabil* **6**, 10-12.
- Benveniste, E. N. (1997) Role of macrophages/microglia in multiple sclerosis and experimental allergic encephalomyelitis. *J Mol Med (Berl)*, **75**, 165-173.
- Cao, L. and He, C. (2013) Polarization of macrophages and microglia in inflammatory demyelination. *Neurosci Bull*, **29**, 189-198.
- Conus, S. and Simon, H. U. (2008) Cathepsins: key modulators of cell death and inflammatory responses. *Biochem Pharmacol*, **76**, 1374-1382.
- David, S. and Kroner, A. (2011) Repertoire of microglial and macrophage responses after spinal cord injury. *Nat Rev Neurosci*, **12**, 388-399.
- Dendrou, C. A., Fugger, L. and Friese, M. A. (2015) Immunopathology of multiple sclerosis. *Nat Rev Immunol*, **15**, 545-558.
- Engelhardt, B. (2006) Molecular mechanisms involved in T cell migration across the blood-brain barrier. *J Neural Transm (Vienna)*, **113**, 477-485.
- Eyles, J. L., Roberts, A. W., Metcalf, D. and Wicks, I. P. (2006) Granulocyte colony-stimulating factor and neutrophils--forgotten mediators of inflammatory disease. *Nat Clin Pract Rheumatol*, **2**, 500-510.

Fan, K., Wu, X., Fan, B., Li, N., Lin, Y., Yao, Y. and Ma, J. (2012) Up-regulation of microglial cathepsin C expression and activity in lipopolysaccharide-induced neuroinflammation. *J Neuroinflammation*, **9**, 96.

Flach, A. C., Litke, T., Strauss, J. et al. (2016) Autoantibody-boosted T-cell reactivation in the target organ triggers manifestation of autoimmune CNS disease. *Proc Natl Acad Sci U S A*, **113**, 3323-3328.

Garcia-Laorden, M. I., Stroo, I., Blok, D. C., Florquin, S., Medema, J. P., de Vos, A. F. and van der Poll, T. (2016) Granzymes A and B Regulate the Local Inflammatory Response during *Klebsiella pneumoniae* Pneumonia. *J Innate Immun*, **8**, 258-268.

Hamilton, G., Colbert, J. D., Schuettelkopf, A. W. and Watts, C. (2008) Cystatin F is a cathepsin C-directed protease inhibitor regulated by proteolysis. *EMBO J*, **27**, 499-508.

Hamon, Y., Legowska, M., Herve, V. et al. (2016) Neutrophilic Cathepsin C Is Matured by a Multistep Proteolytic Process and Secreted by Activated Cells during Inflammatory Lung Diseases. *J Biol Chem*, **291**, 8486-8499.

Hickey, W. F., Hsu, B. L. and Kimura, H. (1991) T-lymphocyte entry into the central nervous system. *J Neurosci Res*, **28**, 254-260.

Hind, L. E., Lurier, E. B., Dembo, M., Spiller, K. L. and Hammer, D. A. (2016) Effect of M1-M2 Polarization on the Motility and Traction Stresses of Primary Human Macrophages. *Cell Mol Bioeng*, **9**, 455-465.

Kummer, J. A., Kamp, A. M., Citarella, F., Horrevoets, A. J. and Hack, C. E. (1996) Expression of human recombinant granzyme A zymogen and its activation by the cysteine proteinase cathepsin C. *J Biol Chem*, **271**, 9281-9286.

Lampron, A., Larochele, A., Laflamme, N. et al. (2015) Inefficient clearance of myelin debris by microglia impairs remyelinating processes. *J Exp Med*, **212**, 481-495.

Liang, J., Li, N., Zhang, Y. et al. (2016) Disinhibition of Cathepsin C Caused by Cystatin F Deficiency Aggravates the Demyelination in a Cuprizone Model. *Front Mol Neurosci*, **9**, 152.

Liu, Y., Hao, W., Letiembre, M., Walter, S., Kulanga, M., Neumann, H. and Fassbender, K. (2006) Suppression of microglial inflammatory activity by myelin phagocytosis: role of p47-PHOX-mediated generation of reactive oxygen species. *J Neurosci*, **26**, 12904-12913.

Ma, J., Tanaka, K. F., Shimizu, T., Bernard, C. C., Kakita, A., Takahashi, H., Pfeiffer, S. E. and Ikenaka, K. (2011) Microglial cystatin F expression is a sensitive indicator for ongoing demyelination with concurrent remyelination. *J Neurosci Res*, **89**, 639-649.

Ma, J., Tanaka, K. F., Yamada, G. and Ikenaka, K. (2007) Induced expression of cathepsins and cystatin C in a murine model of demyelination. *Neurochem Res*, **32**, 311-320.

Martinez, F. O., Helming, L. and Gordon, S. (2009) Alternative activation of macrophages: an immunologic functional perspective. *Annu Rev Immunol*, **27**, 451-483.

McPherson, R. C., Cambrook, H. E., O'Connor, R. A. and Anderton, S. M. (2014) Induction of passive EAE using myelin-reactive CD4<sup>+</sup> T cells. *Methods Mol Biol*, **1193**, 187-198.

Mishina, M. and Sakimura, K. (2007). Conditional gene targeting on the pure C57BL/6 genetic background. *Neurosci Res*, **58**, 105–112.

- Mix, E., Ibrahim, S., Pahnke, J., Koczan, D., Sina, C., Bottcher, T., Thiesen, H. J. and Rolfs, A. (2004) Gene-expression profiling of the early stages of MOG-induced EAE proves EAE-resistance as an active process. *J Neuroimmunol*, **151**, 158-170.
- Nemeth, T., Mocsai, A. and Lowell, C. A. (2016) Neutrophils in animal models of autoimmune disease. *Semin Immunol*, **28**, 174-186.
- Nuro-Gyina, P. K., Rieser, E. L., Granitto, M. C. et al. (2016) Regulation of effector function of CNS autoreactive CD4 T cells through inhibitory receptors and IL-7Ralpha. *J Neuroinflammation*, **13**, 302.
- Pham, C. T. and Ley, T. J. (1999) Dipeptidyl peptidase I is required for the processing and activation of granzymes A and B in vivo. *Proc Natl Acad Sci U S A*, **96**, 8627-8632.
- Robinson, A. P., Harp, C. T., Noronha, A. and Miller, S. D. (2014) The experimental autoimmune encephalomyelitis (EAE) model of MS: utility for understanding disease pathophysiology and treatment. *Handb Clin Neurol*, **122**, 173-189.
- Sano, H., Hsu, D. K., Apgar, J. R., Yu, L., Sharma, B. B., Kuwabara, I., Izui, S. and Liu, F. T. (2003) Critical role of galectin-3 in phagocytosis by macrophages. *J Clin Invest*, **112**, 389-397.
- Sayed, B. A., Christy, A. L., Walker, M. E. and Brown, M. A. (2010) Meningeal mast cells affect early T cell central nervous system infiltration and blood-brain barrier integrity through TNF: a role for neutrophil recruitment? *J Immunol*, **184**, 6891-6900.
- Shimizu, T., Wisessmith, W., Li, J. et al. (2017) The balance between cathepsin C and cystatin F controls remyelination in the brain of Plp1-overexpressing mouse, a chronic demyelinating disease model. *Glia*, **65**, 917-930.

Shresta, S., Graubert, T. A., Thomas, D. A., Raptis, S. Z. and Ley, T. J. (1999) Granzyme A initiates an alternative pathway for granule-mediated apoptosis. *Immunity*, **10**, 595-605.

Sindrilaru, A., Peters, T., Wieschalka, S. et al. (2011) An unrestrained proinflammatory M1 macrophage population induced by iron impairs wound healing in humans and mice. *J Clin Invest*, **121**, 985-997.

Tanaka, K. F., Ahmari, S. E., Leonardo, E. D. et al. (2010) Flexible Accelerated STOP Tetracycline Operator-knockin (FAST): a versatile and efficient new gene modulating system. *Biol Psychiatry*, **67**, 770-773.

Tanaka, K. F., Matsui, K., Sasaki, T. et al. (2012) Expanding the repertoire of optogenetically targeted cells with an enhanced gene expression system. *Cell Rep*, **2**, 397–406.

Wu, F., Cao, W., Yang, Y. and Liu, A. (2010) Extensive infiltration of neutrophils in the acute phase of experimental autoimmune encephalomyelitis in C57BL/6 mice. *Histochem Cell Biol*, **133**, 313-322.

Zamvil, S. S. and Steinman, L. (1990) The T lymphocyte in experimental allergic encephalomyelitis. *Annu Rev Immunol*, **8**, 579-621.

## Figure Legends

Figure 1. Timeline of the study

Diagram illustrates the time course of overall EAE experiment, CatCKD, CatCOE and WT groups. The time points when tissue samples were collected are illustrated: at 1, 2, 3, 4 and 6 weeks after immunization for pilot experiment and 10, 12 and 14 days after immunization for transgenic mice group experiment. Clinical sign was monitored daily.

Figure 2. *CatC*, *CysF* and *c-fms* mRNA expression patterns throughout the course of EAE

The experimental design of MOG-EAE induced paralysis (A). The expression of *CatC* (B1-F1), *CysF* (B2-F2) and *c-fms* (B3-F3) mRNA was examined in MOG-EAE-induced wild type mice at 1, 2, 3, 4 and 6 weeks (A-E) after immunization with MOG peptide (n = 3 per group). ISH was performed on spinal cord sections at the thoracic level using probes for *CatC*, *CysF* and *c-fms* (for microglial activation) and IHC was performed using a rat monoclonal anti-PLP antibody for myelin staining (B4-F4; outlined with red dash line). Clinical signs were observed daily after immunization and a clinical score was recorded: 0 = normal, 1 = limp tail, 2 = hind leg weakness, 3 = paralysis in both hind legs, 4 = complete paralysis in both hind legs and paralysis in one front leg, 5 = moribund or death. The percentage of the demyelinating area was quantified by densitometric analysis using the Image J program and differences between groups are shown graphed (G). Values represent the mean  $\pm$  SEM. A one-way ANOVA test plus Bonferroni's post hoc test were performed for statistical analysis (\* $p < 0.05$ , \*\* $p < 0.01$ , \*\*\* $p < 0.001$  compared between each group). Scale bars: B-F, 200  $\mu\text{m}$ .

Figure 3. *CatC* mRNA-expressing cells infiltrate the spinal cord from the early phase of MOG-EAE

One week after immunizing wild type mice with MOG peptide, the early phase of disease was observed. (A-B) Spinal cord sections at the thoracic level were analyzed by ISH using a *CatC* probe. (C) The image shows the identification of *CatC* mRNA-positive (red arrow heads; blue staining) infiltrating cells as microglia (brown staining) by double labeling for *CatC* by ISH and by IHC using a rabbit anti-Iba1 polyclonal antibody in the anterior gray horn of the spinal cord. (D) Hematoxylin and eosin staining for blood cell identification in the anterior median fissure of the spinal cord. Scale bars: A, 150  $\mu\text{m}$ ; B, 40  $\mu\text{m}$ ; C-D, 20  $\mu\text{m}$ .

Figure 4. *CatC* and *CysF* are expressed in myelin-degenerated areas with active phagocytosis.

MOG-EAE was induced in wild type mice, which were sacrificed 2 weeks after immunization. Myelin phagocytosis was detected by Galectin 3 (Gal3) ISH (A) and

demyelinated area detected by PLP IHC (B; outlined with red dash line in A as well). Spinal cord sections at the thoracic level were analyzed by ISH using probes for *CatC* (C) or *CysF* (D). Scale bars: A-B, 200  $\mu\text{m}$ ; D-C, 100  $\mu\text{m}$ .

Figure 5. pro-inflammatory damaging (M1) or anti-inflammatory neuroprotective (M2) polarization of Microglia/Macrophages in MOG-EAE

MOG-EAE was induced in wild type mice, which were sacrificed 6 weeks after immunization. Spinal cord cryosections at the thoracic level were analyzed by IHC using a rat monoclonal anti-CD16/32 antibody for damaging microglial cells (A; yellow arrow head, red staining) or a goat polyclonal anti-Arginase1 (ARG-1) antibody for neuroprotective microglial cells (D; yellow arrow heads, red staining) followed by nuclear staining with Hoechst (B, E). Merged images are shown (C, F). Scale bar: 50  $\mu\text{m}$ .

Figure 6. *CatC* gene manipulation affects the clinical severity of MOG-EAE

The clinical score of *CatC*<sup>STOP/STOP</sup> (CatCKD) and wild type (WT) mice (A), and *CatC*<sup>STOP/STOP</sup>*Iba*<sup>TA/-</sup> (CatCOE) and WT mice (B), in which MOG-EAE was induced and animals were sacrificed 2 weeks after immunization, was measured daily after immunization and recorded: 0 = normal, 1 = limp tail, 2 = hind leg weakness, 3 = paralysis in both hind legs, 4 = complete paralysis in both hind legs and paralysis in one front leg, 5 = moribund or death. Six independent experiments were performed with a total number of 13 CatCKD, 12 CatCOE and 15 WT animals to obtain clinical score at the various time points. Values represent the mean  $\pm$  SEM. A two-Way ANOVA test plus Bonferroni's post hoc test were performed for statistical analysis (\* $p < 0.05$ , \*\* $p < 0.01$ , \*\*\* $p < 0.001$  compared to the control group).

Figure 7. *CatC* gene manipulation affects demyelination after MOG- EAE

MOG-EAE was induced in CatCKD (n = 3) (A), CatCOE (n = 4) (B) and wild type (n = 4) (C) mice, and animals were sacrificed 2 weeks after immunization. Spinal cord sections at the thoracic level were analyzed by ISH using probes for *CatC*, *CysF* or *c-fms* (for

microglial activation), and by IHC using a rat monoclonal anti-PLP antibody for myelin staining (outlined with red dash line). The percentage of the demyelinating area was quantified by densitometric analysis using the Image J program and differences between groups are shown graphed (D). Values represent the mean  $\pm$  SEM. An unpaired two-tailed Student's *t*-test was performed for statistical analysis ( $*p < 0.05$  compared with the control group). Scale bars: A-C, 200  $\mu\text{m}$ .

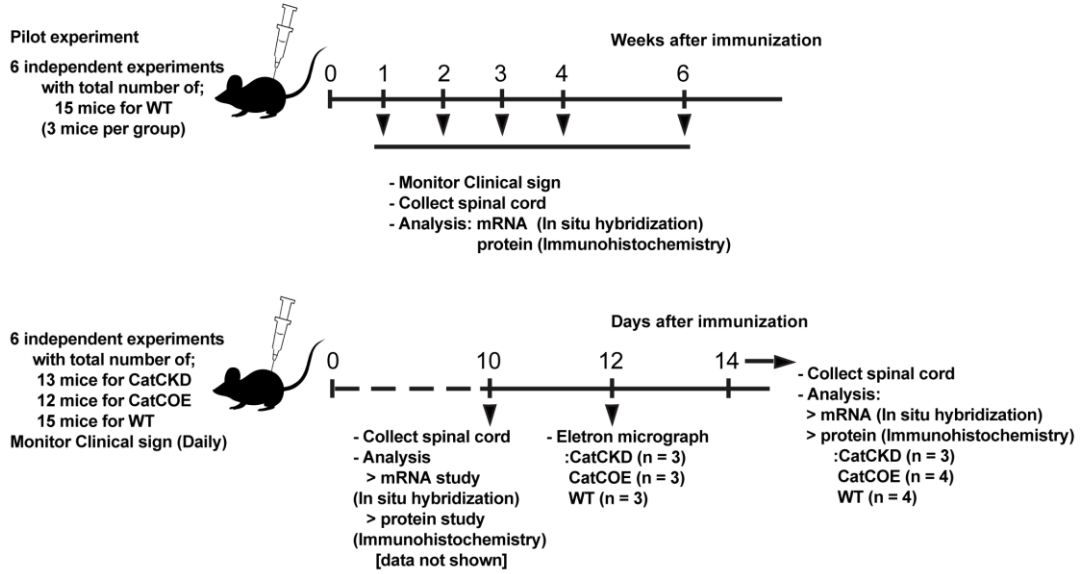
Figure 8. Neutrophil infiltration into the CNS in *CatC*-overexpressing mice.

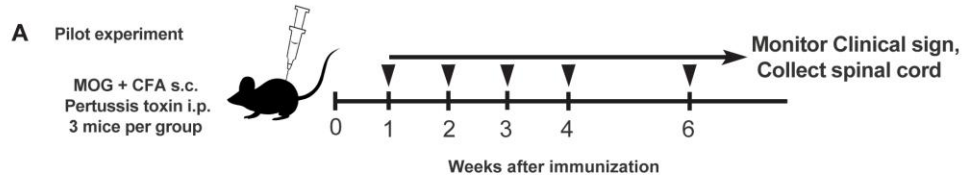
Electron micrographs of wild type (A, D), CatCKD (B, E) and CatCOE (C, F) mice in which MOG-EAE was induced and animals were sacrificed 12 days after immunization.

Multinuclear neutrophilic cells were observed (C, F; black arrow). The average number of invading cells under a  $\times 2000$  magnification field was quantified and differences between groups are shown graphed (G). Scale bars: A-C, 5  $\mu\text{m}$ ; D-F, 1  $\mu\text{m}$ .

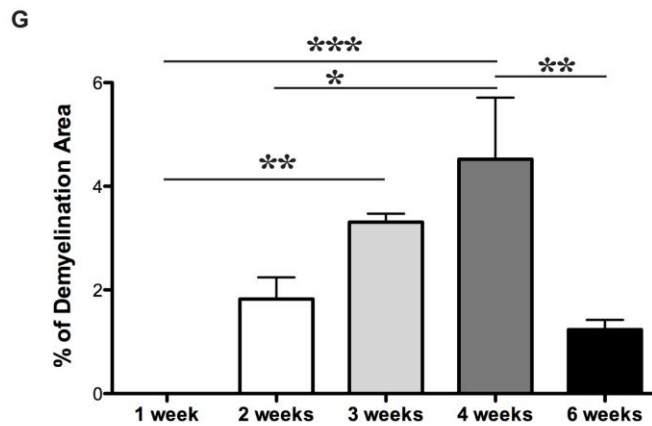
### Overview of Study Design Experiments

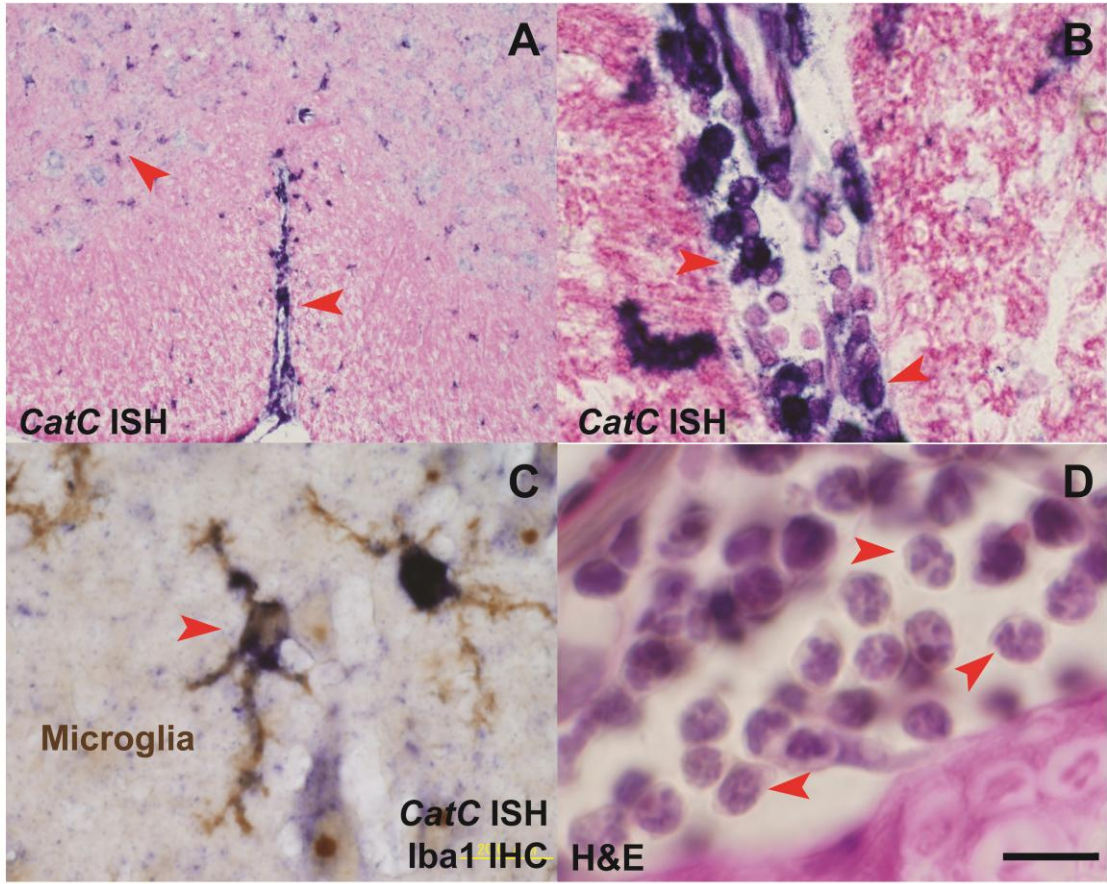
Experiment: MOG35-55 peptide in CFA + IFA (1:1) s.c.  
 Pertussis toxin i.p.

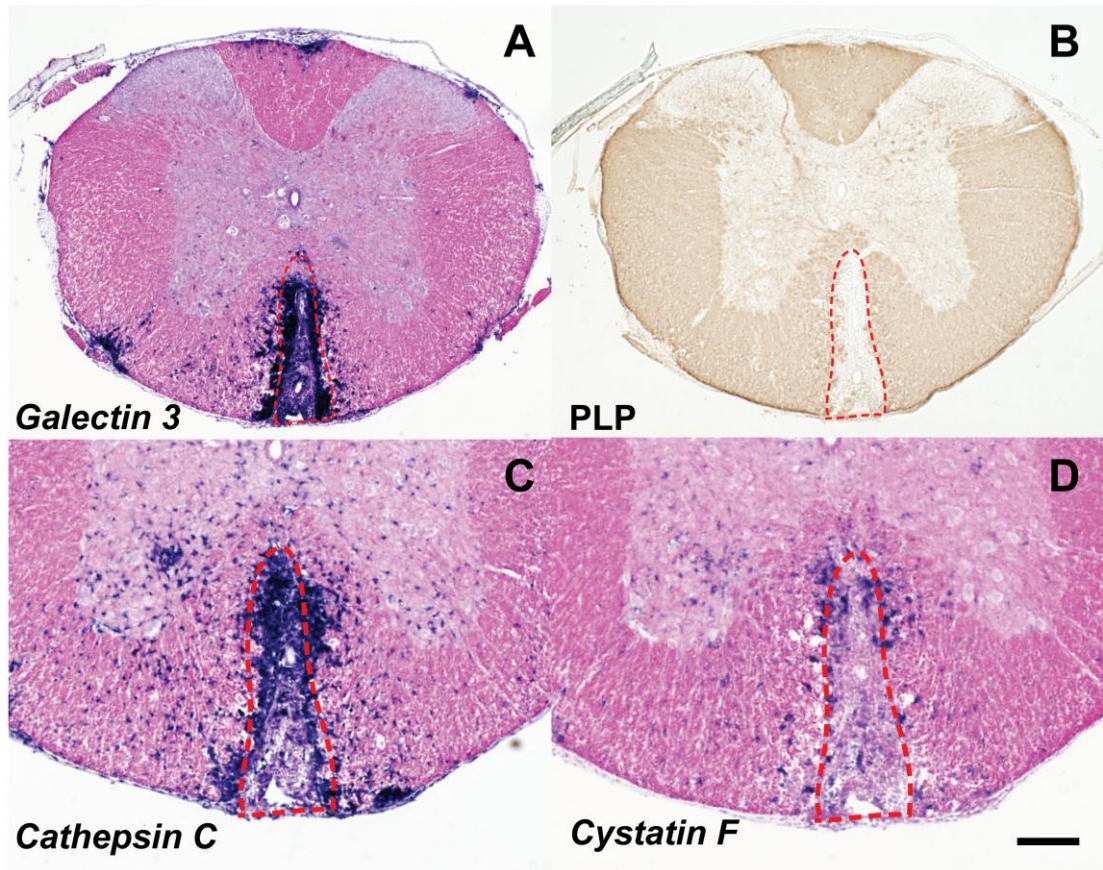


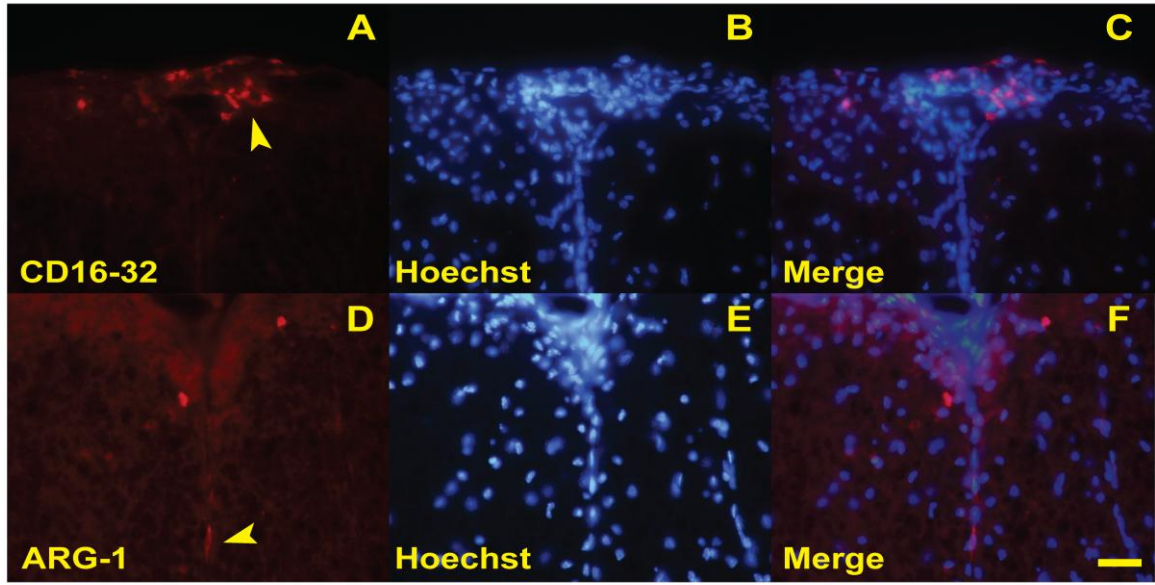


|         | <i>CatC</i> ISH | <i>CysF</i> ISH | <i>c-fms</i> ISH | PLP IHC | Clinical Symptom  |
|---------|-----------------|-----------------|------------------|---------|---|
| 1 week  | B1              | B2              | B3               | B4      | None<br>(CS = 0)  |
| 2 weeks | C1              | C2              | C3               | C4      | Impaired righting reflex, Incomplete hindlimb paralysis<br>(CS = 2/3) |
| 3 weeks | D1              | D2              | D3               | D4      | Hindlimb paralysis<br>(CS = 3/4)                                      |
| 4 weeks | E1              | E2              | E3               | E4      | Fore and Hind limb paralysis or moribund<br>(CS = 3/4/5)              |
| 6 weeks | F1              | F2              | F3               | F4      | Recovery phase<br>Regain function<br>(CS = 2/1)                       |

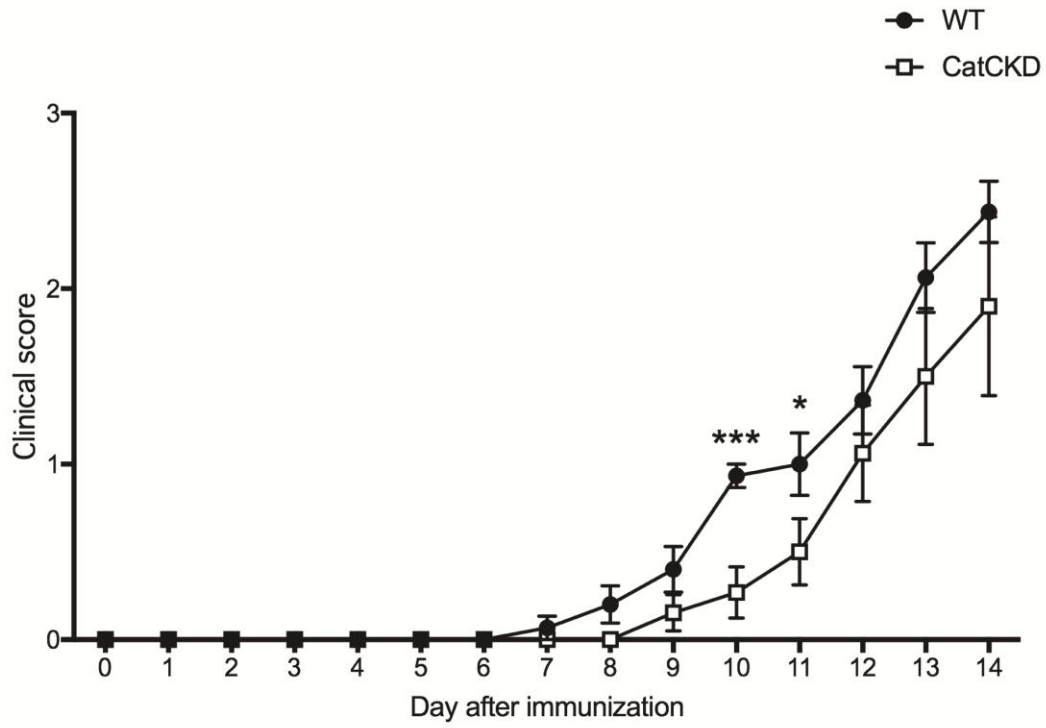




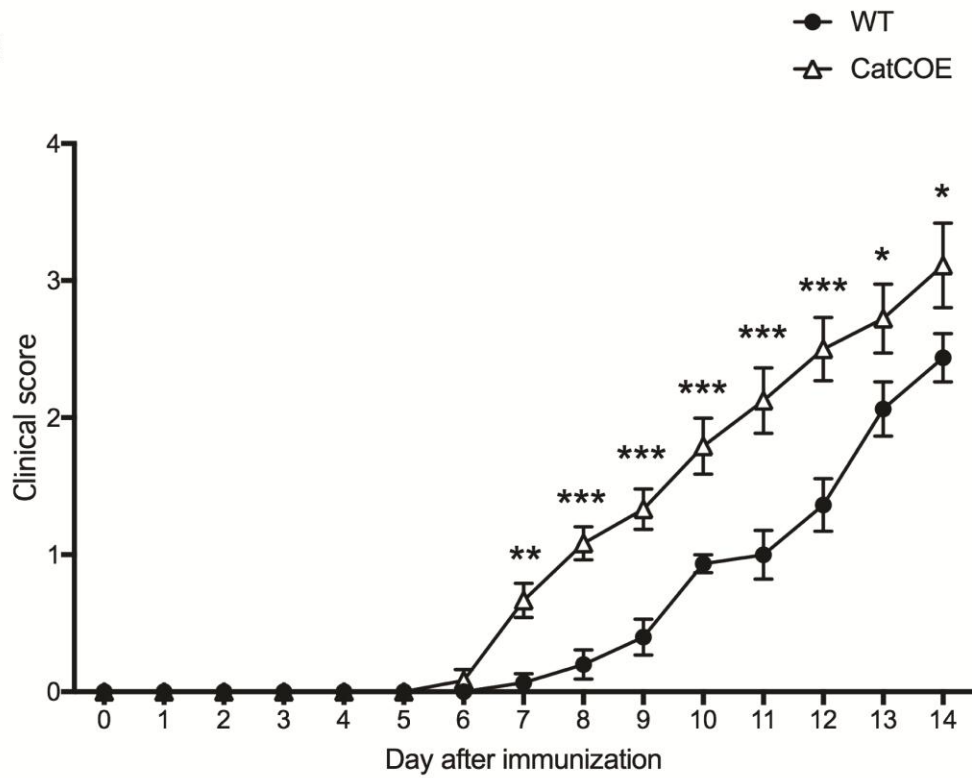


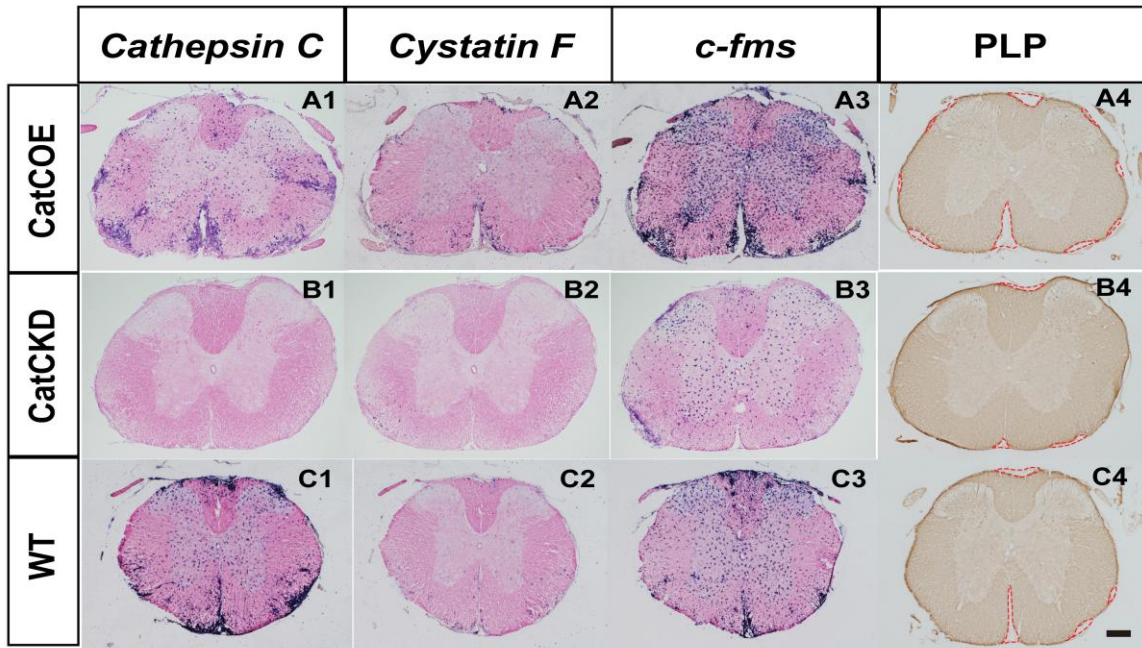


**A**



**B**





D

